



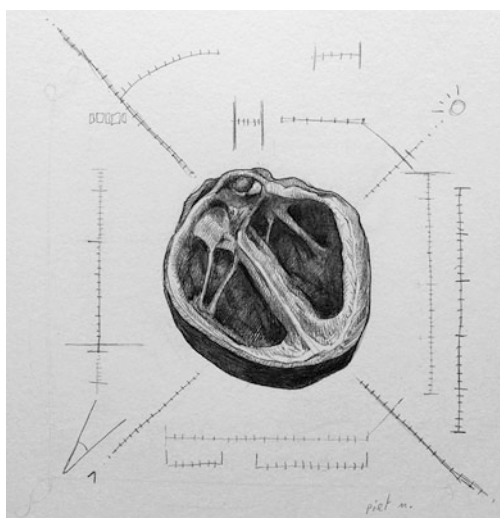


Cardiophysiology Illustrated by Comparing Ventricular Volumes in Healthy Adult Males and Females

8

Peter L. M. Kerkhof , Tatiana Kuznetsova , J. Yasha Kresh ,
and Neal Handly 



Assessment of cardiac size. Art work by Piet Michiels, Leuven, Belgium.

P. L. M. Kerkhof (✉)

Department of Radiology and Nuclear Medicine,
Amsterdam Cardiovascular Sciences, VU University
Medical Center, Amsterdam, The Netherlands
e-mail: plm.kerkhof@vumc.nl

T. Kuznetsova

Department of Cardiovascular Sciences, University of
Leuven, Leuven, Belgium

J. Yasha Kresh

Departments of Cardiothoracic Surgery and Medicine
(Cardiology), Drexel University College of Medicine,
IME, University of Pennsylvania, Philadelphia, PA, USA

N. Handly

Department of Emergency Medicine, Drexel University
College of Medicine, Philadelphia, PA, USA

Abstract

Recent advances in cardiac imaging techniques have substantially contributed to a growing interest in the analysis of global cardiac chamber dimensions and regional myocardial deformation. During the cardiac cycle, ventricular luminal volume varies due to the contraction process, which also confers a shape change including substantial alteration of long axis length, as well as rotation of the base compared to the apex. Local deformation can be assessed by strain (rate) analysis. Reviewing the present literature, it must be concluded that there is no single metric

available to comprehensively characterize ventricular function. Every candidate advanced thus far has been found to incompletely reflect ventricular performance. This observation is not surprising in view of the complexity of the cardiac pump system. Additionally, sex-specific modifiers may play a role. More than three decades ago, it was shown that on average the ventricular volume is smaller in healthy women compared to matched males. Therefore, the present contribution concerns the interpretation of data derived from the healthy heart in both men and women. Starting from the classical Starling concept, we apply a simple mathematical transformation which permits an insightful representation of ventricular mechanics. Relating end-systolic volume (ESV) to end-diastolic volume creates the ventricular volume regulation graph which features the pertinent working point of an individual heart. This fundamental approach illustrates why certain proposed performance indexes cannot individually reveal the essence of ventricular systolic function. We demonstrate that particular metrics are highly interconnected and just tell us the same story in a different disguise. It is imperative to understand which associations exist and if they expectedly are (nearly) linear or frankly nonlinear. Notably, ejection fraction (EF) is primarily determined by ESV, while in turn EF is not much different from ventriculo-arterial coupling (VAC). Insight into cardiac function is promoted by identification of the paramount/essential components involved. The smaller ESV ($p < 0.0001$) implies that EF is higher in women and may also have consequences for VAC.

Keywords

Ventricular volume · Sex-specific analysis · Starling concept · Ejection fraction · Cardiac output · Heart rate · End-systolic volume · Systolic elastance · Ventriculo-arterial coupling · Pressure–volume loop · History of cardiology · Titin isoforms · Soltis–Saucerman model · Cardiomyogenesis · Review

Introduction

Gross anatomical contours of the heart have been depicted already by prehistoric hunters more than 17,000 years ago (the Upper Paleolithic period). Examples of such primitive art have been found in the caves of Lascaux, Southern France. One view holds that these instructional paintings facilitated the work of hunt; another refers to an expiatory ritual [4]. Until the late Middle Ages, most anatomical illustrations concern the complete body, without attention for individual organs [45]. The first illustrated anatomical textbook that includes a detailed description of the structure of the heart was written by Jacopo Berengario (Barigazzi) of Carpi [23, 47]. His insights were based on the many dissections performed when he was professor of surgery at Bologna between 1502 and 1527 [53]. The transition from anatomy (i.e. form) to physiology (*viz.* pump function) took several centuries. It must be emphasized that determination of the phasic size of the beating heart was not relevant until relatively recently (i.e., around 1900), when physiologists started studying pump function, e.g., by relating output to input (see Frank & Starling). Even William Harvey [14] was not primarily interested in ventricular size as such. He just mentioned an estimate of the amount of circulating blood by stating that everyone who crosses streets in the butchers' quarter knows that only a few liters of blood leave the animal once the major neck vessels are severed. It was more than a century later that interest developed in quantifying the size of the (non-beating) heart. Investigations regarding left ventricular (LV) size and shape were carried out by the Reverend Stephen Hales (1677–1761) from Middlesex, who made casts of the lumen of animal heart chambers using the beeswax cast technique [13]. A recently created example based on the same technique is shown in a photographic illustration elsewhere [26].

Cardiac function has often been analyzed by evaluating cardiac output (CO), as well as by considering metrics that directly employ information on end-systolic volume (ESV) and end-diastolic volume (EDV). An indication about the

magnitude of CO in animals was noted by Harvey, as mentioned. Following experiments on skeletal muscle, cardiac physiologists commenced investigating the isolated animal heart, while manipulating filling characteristics as in the experiments by O. Frank, E. Starling, and M. Blix [15, 49]. Around the beginning of the twentieth century, physiologists analyzed the relationship between filling (preload) and output, resulting in the famous Starling curve. The Italian scientist Dario Maestrini (Corciano 1886–1975 Arezzo) is said to have arrived at similar statements [36, 38]. It took somewhat longer to devise methods that can actually estimate LV chamber volume in the beating intact (innervated) heart. The introduction of indicator dilution techniques permitted calculation of ejection fraction (EF), being the rate of washout during successive heart beats, i.e., ejected stroke volume (SV) relative to filling volume. With the advent of x-ray imaging, biplane angiography, and radio-nuclide tracers, besides noninvasive methods such as advanced 3D echocardiography, MRI, and CT scan, accurate estimations of ESV and EDV became within reach [31]. Thus, EF became “redefined” as $(1-ESV/EDV)$. The distinction between ventricular size in men and women was established 35 years ago [7, 8] and is increasingly being appreciated.

Cardiomyocyte and Contraction Process

The fundamental building block of cardiac muscle contraction refers to the cardiomyocyte which contains myofibrils consisting of contractile proteins arranged in units which are called sarcomeres. Activation takes place via an electrical stimulus which in the healthy heart spreads from the sinus node via the AV node and the ventricular septum in the direction of the apex, to continue along the free wall in the direction of the base of the heart [24]. The electrical trigger initiates contraction, and the complete sequence can be recorded as the typical electrocardiogram (ECG). The precise mechanisms of contraction at the cellular level are complex and still an area of

intense investigation. The contractile machinery is summarized in Fig. 8.1 [39]. The intrinsic capability to contract and generate force is referred to as contractility (or inotropy). Similarly the property describing the ease of relaxation during diastole is referred to as lusitropy. Both processes are modulated by β -adrenergic stimulation (β -AS), which increases (the rate of) peak force development, in addition to enhancing lusitropy [44]. Notably, β -AS raises intracellular cAMP levels, activating protein kinase A (PKA), which in turn phosphorylates key proteins involved in excitation–contraction (EC) coupling. These include the L-type Ca^{2+} channel and phospholamban (PLB), respectively, increasing Ca^{2+} entry into the cytoplasm and sarcoplasmic reticulum (SR) Ca^{2+} reuptake by the SR Ca^{2+} -ATPase2a (SERCA2a). These effects contribute to increased SR Ca^{2+} content, inotropy, and lusitropy. High SR Ca^{2+} load also enhances Ca^{2+} leak and fractional Ca^{2+} release during EC coupling. Interestingly, β -AS has been shown to increase the gain of cardiac EC coupling. Mechanisms of cardiac EC coupling have been found to differ between the sexes [10]. Contractions and Ca^{2+} transients in rats are significantly smaller in myocytes from females when compared to males. Ca^{2+} spark frequency does not differ between the sexes, but amplitudes are smaller in cells from females when compared to males. Thus, the gain of EC coupling (i.e., SR Ca^{2+} release per unit Ca^{2+} current) is much lower in cells from females [10]. As the amount of Ca^{2+} released during a spark is regulated by the intrinsic gating of the RyR2 (type 2 release) channels, sex differences in the opening of individual channels could be responsible. Alternatively, as RyR2 levels are actually higher in females, it is possible that there are posttranslational modifications in males that could contribute to increased SR Ca^{2+} release by increasing channel opening [40]. Additionally, estrogen receptor activation was found to influence cardiac myofilament function [33]. At the myofilaments, PKA phosphorylates troponin I (TnI) and myosin binding protein-C (MyBP-C). Cross-bridge (XB) cycling rate (XBcy) is still debated in the literature. Most studies on ion channels and Ca^{2+} transport

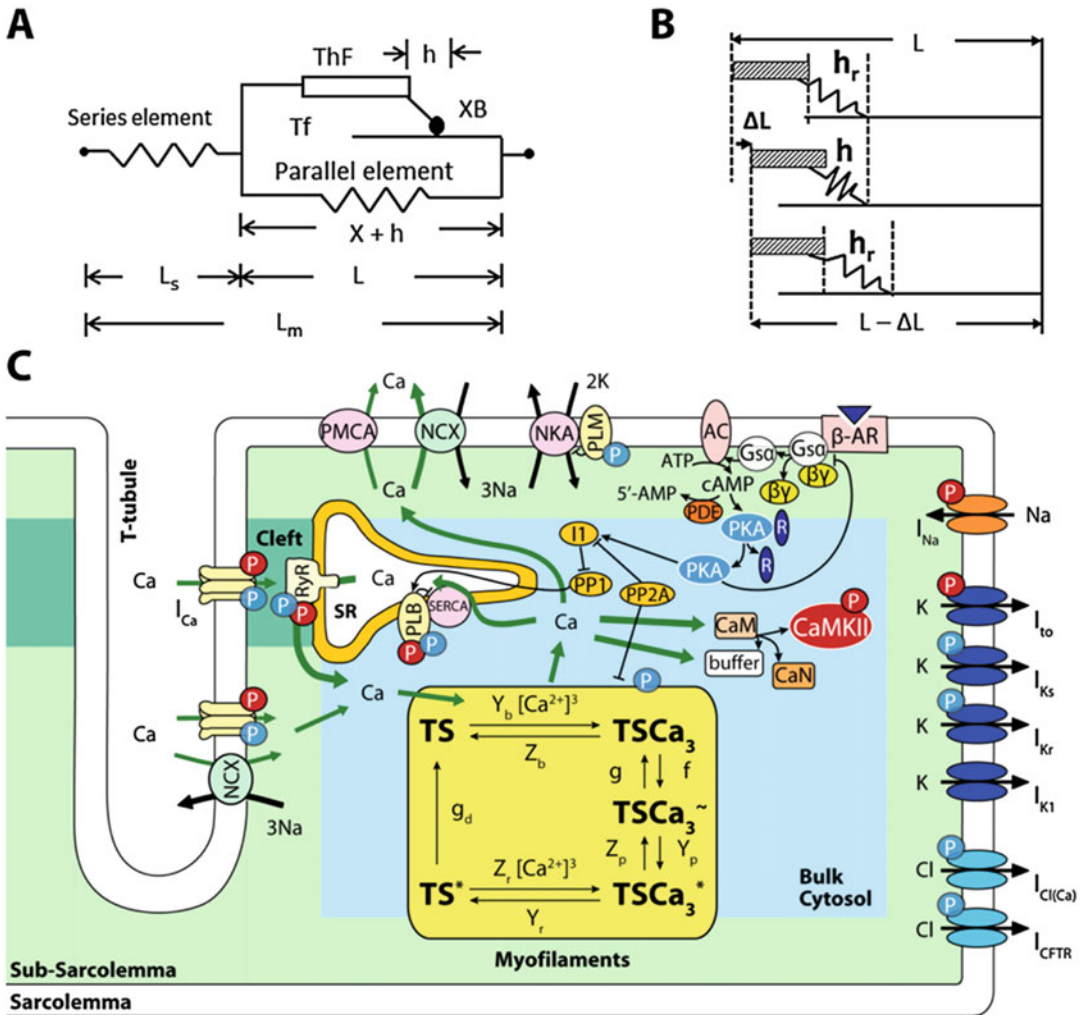


Fig. 8.1 Model summarizing major components and processes involved in cardiac contraction at the cellular level (A) Constitutive muscle unit, consisting of half-sarcomere length (L) composed of thick (ThF) and thin (Tf) filaments in parallel with an elastic element. The equivalent cross-bridge (XB) representing all attached cross-bridges is part of the ThF. It attaches to the Tf by the mobile end of its elastic structure, with h elongation, defining an inextensible half-sarcomere length $X = L - h$. A series elastic element with length L_s accounts for compliant muscle ends and together with L make up total muscle length (L_m). (B) Cross-bridge dynamics showing steady-state XB elongation (h_r), its decrease due to ΔL , and later return to h_r at shorter half-sarcomere length ($L - \Delta L$). (C) Four-compartment myocyte model: bulk cytosol, cleft, sarcoplasmic reticulum (SR), and subsarcolemmal space (Sub-SL) [50, 54] with ion currents as described by various authors. This model is coupled to the myofilament force development model consisting of 5-state troponin systems (TS) with Ca^{2+} binding. Each TS is

composed of three adjacent troponin-tropomyosin regulatory units able to act cooperatively to bind Ca^{2+} in three successive steps. Troponin systems are free TS, Ca^{2+} bound to TS without attached XBs (TSCa₃), Ca^{2+} bound to TS with attached XBs in the weak state (TSCa₃[~]), Ca^{2+} bound to TS with attached XBs in the power state (TSCa₃^{*}), and TS without Ca^{2+} with attached XBs in the power state (TS^{*}). Baseline mechanical parameters and all changes used for ISO are in Table 8.1 of the original publication. Reproduced from Negroni et al. [39], with permission. Other abbreviations: AP(D) action potential (duration), CaMKII Ca^{2+} /calmodulin-dependent protein kinase II, CFTR cystic fibrosis transmembrane conductance regulator, EC excitation-contraction, Fm muscle force, ICaL L-type Ca^{2+} channel current, ICFTR CFTR-mediated Cl^- current, ICl(Ca) Ca^{2+} -dependent Cl^- current, IKr rapid delayed rectifier K^+ current, IKs slow delayed rectifier K^+ current, INa fast Na^+ current, INCX Na^+ - Ca^{2+} exchanger current, INKA Na^+ - K^+ -ATPase current, ISO isoproterenol, ISO-Cytofl ISO effect without

have been limited to myocyte ion handling and electrophysiological descriptions. However, an advanced approach by Negroni et al. [39] clarifies how altered Ca^{2+} sensitivity and XBcy interact during β -AS in ventricular myocytes. Thus, they provide a quantitative framework to study β -AS dynamic effects on Ca^{2+} transients, action potential, and contractile properties while incorporating an updated Soltis–Saucerman model [54]. The latter integrates the Shannon–Bers Ca^{2+} electrophysiological myocyte model [50] with dynamic descriptions of CaMKII and PKA signaling pathways. The half-sarcomere is composed of inextensible thick and thin filaments in parallel with an internal elastic load (Fig. 8.1a). The thick (ThF) and thin filaments (Tf) can slide past each other defining a zone of overlap where XBs can attach to the thin filament. Attached XBs act as independent force generators, occupying different states in the XB cycle [19]. It was demonstrated [15] that as the sarcomere shortens below slack length, titin-based restoring forces act to desensitize the myofilaments. That study showed for the first time the importance of titin-based restoring force in length-dependent deactivation during the early phase of diastole. Titin is synthesized as either the more compliant (fetal) N2BA or stiffer (adult) N2B form. Signaling by thyroid hormone, insulin, and Gq-protein-coupled receptors to the phosphoinositol 3 kinase–Akt–mammalian target of rapamycin pathway enhances N2B expression. The N2BA:N2B ratio generally increases in humans with heart failure (HF) and reduced EF, but changes in patients with preserved EF remain

less certain [51]. Recently, a validation was realized of an LV finite element model driven by a cell-based cross-bridge cycling descriptor and coupled to a closed-loop lumped parameter circulatory model to simulate different ventricular loading conditions (preload and afterload) and contractility levels. This approach permitted reproduction of a linear end-systolic pressure–volume relationship, a curvilinear end-diastolic pressure–volume relationship, and a linear relationship between myocardial oxygen consumption and pressure–volume area [52].

Sex-Specific Differences in Cardiomyocytes

The observation that receptors for all major sex steroid hormones, including testosterone, are present on individual cardiomyocytes suggests that these hormones may influence the heart at the cellular level. Male/female differences in intracellular Ca^{2+} release and contraction in isolated ventricular myocytes have already been mentioned. Growing evidence suggests that these differences arise from effects of sex steroid hormones on processes involved in intracellular Ca^{2+} homeostasis [2]. Also in adult mammals, sex-based differences in cardiac structure and function have been reported, based on main molecular mechanisms involved in the response of the heart to pathological situations. These differences should be dealt with, not only in basic science or clinical research but also with



Fig. 8.1 (continued) β -AS on parameters involved in cytosolic fluxes, *ISO-titin* ISO effect without β -AS on parameters involved in titin, *ISO-XBCa* ISO effect without β -AS on parameters involved in XBCa, *ISO-XBCa–XBcy* ISO effect without β -AS on parameters in XBCa and XBcy, *ISO-XBcy* ISO effect without β -AS on parameters involved in XBcy, *kdf* rate of force redevelopment (as response to a length step), *krel* rate of force decay, *ktr* rate of force redevelopment (response to a length pulse), *Lm* muscle length, *MyBP-C* myosin binding protein-C, *NCX* Na^+ – Ca^{2+} exchanger, *NKA* Na^+ – K^+ -ATPase, *PKA* protein kinase A, *PLB* phospholamban, *PLM*

phospholemman, *PMCA* plasma membrane Ca^{2+} ATPase, a transport protein in the plasma membrane, *RyR* ryanodine receptor, *SERCA* sarcoplasmic reticulum Ca^{2+} -ATPase, *SR* sarcoplasmic reticulum, *TnC* troponin C, *TnI* troponin I, *TSCa3* Ca^{2+} bound to troponin system without attached XBs, *TSCa3* $\sim \text{Ca}^{2+}$ bound to troponin system with attached XBs in the weak state, *TSCa3** troponin system without Ca^{2+} with attached XBs in the power state, *XB* (myofilament) cross-bridge, *XBCa* XB Ca^{2+} sensitivity, *XBcy* cross-bridge cycling rate, *WT* wild type, β -AS β -adrenergic stimulation

regard to therapeutic approaches [11]. Recently, in rats contractility in the whole heart, adult ventricular myocytes, as well as myofibrils from both sexes were analyzed. Functional sex differences were observed at all levels. Hearts and cardiomyocytes from female rats displayed greater fractional shortening (FS) than males, and female cells and myofibrils took longer to relax. RNA sequencing experiments on these cardiomyocytes were performed, resulting in the identification of around 600 genes which were expressed in a sexually dimorphic manner. Further analysis revealed sex-specific enrichment of signaling pathways and key regulators. At the protein level, female cardiomyocytes exhibited higher PKA activity, consistent with pathway enrichment identified through RNA sequencing [56]. In contrast, Farrell et al. [10] found FS to be significantly smaller in female rats, and a similar finding for EF was attributed to the load dependence of the metric. However, one would

rather expect an increased EF level [32] in women in view of the lower arterial blood pressure levels seen in both healthy humans (Table 8.1) and animals [57]. Additionally, it is important to point out that sex differences in genes and gene families often reverse by sex in diseased versus control, healthy tissues [9].

It remains unclear how these differences as observed in rodents translate to macroscopic distinctions in humans. Reportedly, EF is higher in women ([8], and also this study), but the observation is likely associated with their smaller ESV values [30]. Differences also occur during aging. A progressive loss of telomeric DNA in human cardiac stem cells (hCSCs) occurs with aging, and the newly formed cardiomyocytes inherit short telomeres and rapidly reach the senescent phenotype. One study including female ($N = 32$) and male ($N = 42$) hearts from individuals without cardiovascular disease (age range 19–104 years) demonstrated that at all ages, the female heart is

Table 8.1 Hemodynamic variables in healthy adults ($N = 410$) based on Kuznetsova et al. [34]

Variable	Women		Men	<i>p</i> -value	Unit
Persons involved	215		195		number
Age	43.4	≈	42.7	0.62	years
Systolic blood pressure	116.5	<	121.8	<0.0001	mmHg
Diastolic blood pressure	74.6	<	77.8	<0.0001	mmHg
Mean arterial pressure	88.6	<	92.5	<0.0001	mmHg
End-systolic volume index	17.7	<	22.5	<0.0001	mL/m ²
End-diastolic volume index	48.7	<	59.3	<0.0001	mL/m ²
Stroke volume index	31.0	<	36.8	<0.0001	mL/m ²
Cardiac output index	1.93	<	2.13	<0.0001	L/min.m ²
Ejection fraction	63.7	>	61.9	0.0026	%
Effective arterial elastance	2.97	>	2.62	<0.0001	mmHg.m ² /mL
E _{max} (assuming V ₀ = 0)	5.3	>	4.3	<0.0001	mmHg.m ² /mL
Ventriculo-arterial coupling	1.83	>	1.69	0.003	dimensionless
Arterial compliance	0.77	<	0.86	<0.0001	mL/(mmHg.m ²)
Pulse pressure	41.9	<	44.0	0.009	mmHg
Peripheral resistance	48.1	>	45.4	0.014	mmHg.min.m ² /L
Body surface area	1.74	<	1.97	<0.0001	m ²
Heart rate	62.5	>	58.6	<0.0001	beats/minute

Volume data obtained by 2D echocardiography, collected in a north-eastern region of Belgium with mostly Caucasian inhabitants (including 215 women). The subgroup listed here excludes individuals with hypertension or diabetes mellitus. Possible age-dependent variation has not been considered in this survey. Note that all variables (with the exception of age) are significantly different in females when compared to males. In summary: pressures are lower in healthy women, while their ventricular volumes are smaller. E_{max} and V₀ are defined in Fig. 8.3, assuming that V₀ vanishes. Details on standard deviations have been omitted for simplicity.

equipped with a larger pool of functionally competent hCSCs and younger myocytes than the male myocardium. The replicative potential is higher, and telomeres are longer in female hCSCs than in male hCSCs. In the female heart, myocyte turnover occurs at a rate of 10%, 14%, and 40% per year at 20, 60, and 100 years of age, respectively. Corresponding values in the male heart are 7%, 12%, and 32% per year, documenting that cardiomyogenesis involves a large and progressively increasing number of parenchymal cells with aging. From 20 to 100 years of age, the myocyte compartment is replaced 15 times in women and 11 times in men [20].

Ventricular Pressure and Volume in Males and Females

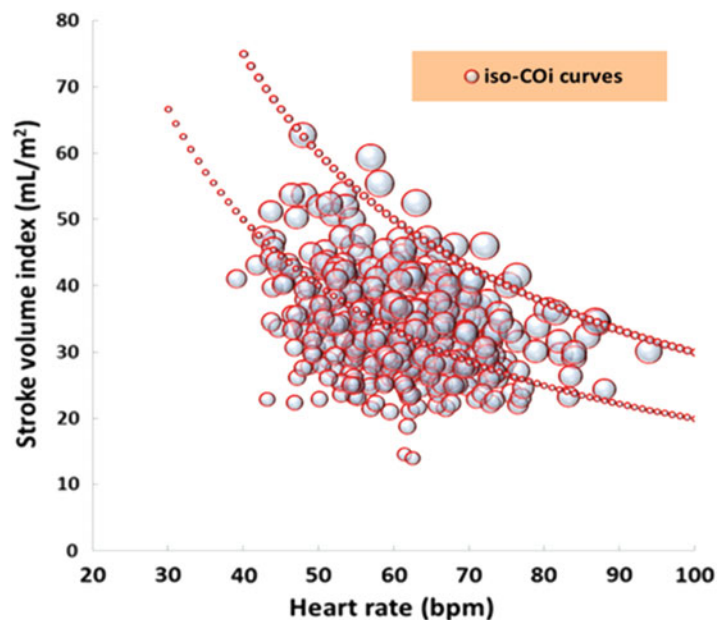
So much for the difficult part. All those ion currents and sliding filament activities serve to get something like a compression pump fully operational on a 24-h basis. Now the more straightforward pump function description deserves attention, referring to a macroscopic view. Stroke volume (SV) and heart rate (HR) are important determinants of ventricular pumping capacity. SV

is the difference between EDV and ESV. Cardiac output (CO) is obtained by multiplying SV and HR. Figure 8.2 illustrates positions of SV and HR combinations as measured in a population consisting of 410 healthy individuals. Iso-CO curves (i.e., trajectories with fixed CO levels) are inscribed. Obviously, similar values for SV can be generated by various suitable combinations of EDV and ESV. Therefore, we need a framework in which we can depict not just the difference between EDV and ESV (as shown on the ordinate of Fig. 8.2), but rather the particular volumes that actually generate a certain SV, either in a healthy individual or in a cardiac disease patient. In other words, it is required to define a so-called working point, which exactly characterizes the conditions which are responsible for a particular SV. This concept has been presented in detail elsewhere [32].

The Pressure–Volume Loop in Healthy Males and Females

Table 8.1 shows a comparison of various hemodynamically relevant variables routinely explored in clinical investigations. Apart from the slight

Fig. 8.2 Diagram showing combinations of stroke volume index and heart rate as measured in 410 healthy adults. Multiplication of both components yields cardiac output index (COi), as reflected by the relative bubble size. Two levels of constant COi are indicated by the dotted curves, namely 3 (upper tracing) and 2 L/min.m². Average values are different for males and females (see Table 8.1). Abbreviation: bpm, beats per minute



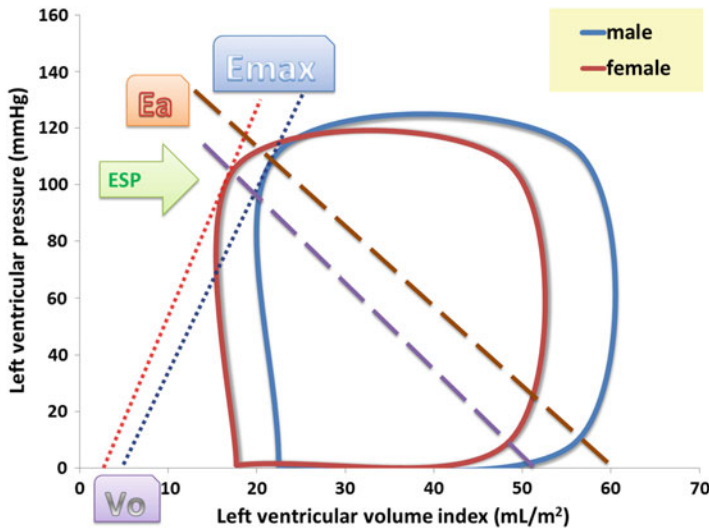


Fig. 8.3 Schematic sketch of the left ventricular pressure–volume loop, reflecting the dynamic behavior during a single cardiac cycle. Although not emphasized in most textbooks, there are considerable differences between the healthy adult male and female. The loops refer to a single cardiac cycle. Filling is complete when reaching end-diastolic volume (EDV). Then pressure builds up, which eventually opens the aortic valve, while starting ejection until end-systolic volume (ESV) with end-systolic pressure (ESP) is reached. Subsequently

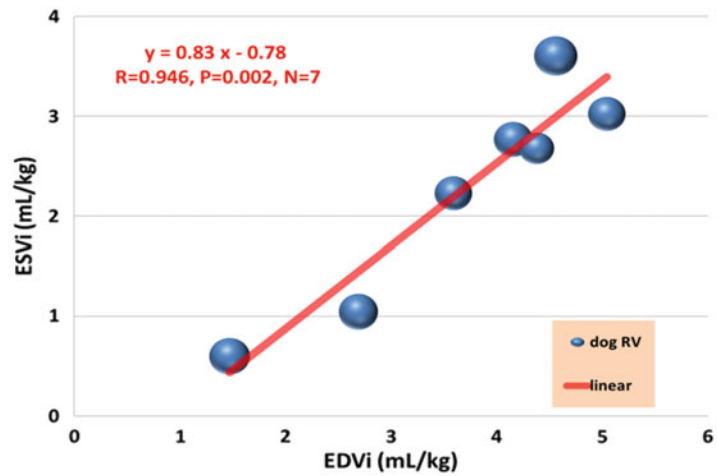
pressure falls and filling resumes. Essentially the diagram is similar for men and women, except for the fact that ESV and EDV are significantly smaller in healthy adult women, while ESP is slightly lower. End-systolic elastance E_{max} is defined as $ESP / (ESV - V_0)$, where V_0 is an extrapolated value, here based on a reasonable estimate. The effective arterial elastance (E_a) is given by $ESP / (EDV - ESV)$. The ratio of E_{max} and E_a is called ventriculo-arterial coupling. Based on average data from [34] see Table 8.1

disparity of systolic pressure, it is remarkable to observe the significant differences regarding LV volumes when comparing men and women. This notable fact was first published by Buonanno et al. [8] and unfortunately had not received the attention which it deserves. Figure 8.3 combines LV pressure and volume data to construct average PV loops, typical for healthy males and females. Again, the contours of the loops depict remarkable sex-specific differences which generally are not discussed in standard textbooks. The LV peak systolic pressure (PSP) vs ESV relationship was first described by Holt [17]. Nowadays, end-systolic pressure (ESP) is often approximated as $0.9 \cdot PSP$, yielding the familiar maximal systolic elastance (E_{max}), shown in Fig. 8.3.

It is well-known that the size of the healthy heart varies, depending on age and size of the animal or human under consideration. In contrast, in the healthy organism, it is found that arterial

blood pressure at resting conditions is nearly constant across all species, although being slightly lower in adult healthy females [48, 57]. A popular index to indicate systolic function (i.e., pump performance) is EF, being the ratio of SV and EDV and often expressed as a percentage. Since average ESV is significantly smaller in healthy adult women, it follows that EF tends to be higher in females [30], and this is confirmed (Table 8.1) based on data described elsewhere [34]. Although EF depends on both ESV and EDV, it appears that ESV is the dominant component [30]. Indeed, the relationship between EF and ESV is based on the boundary conditions of ventricular function, where ESV cannot be greater than EDV, while values for SV occur within a certain range. When these restrictions are applied to a Monte Carlo model, we find a distribution of theoretical working points similar to what we encounter in the actual VRG [27]. In Fig. 8.3 the SV can be

Fig. 8.4 Volume regulation graph, constructed on the basis of right ventricular (RV) volume data (normalized by body weight) for seven anesthetized dogs as reported by Holt [18], using an electrical conductance method and saline injection to obtain indicator dilution curves. Bubble size refers to heart rate (range 70–108 beats per minute)



identified as the width of the loop, since this is the difference between EDV and ESV. The latter two variables determine the working point as illustrated in Fig. 8.4 which is based on the pioneering work by Holt on obtaining LV and right ventricular (RV) volume in dogs [16–18]. The electric conductivity method employed by those authors to measure volumes was refined [3] and adapted for use in humans, horses [22], and small animals (survey in [31]).

The Volume Regulation Graph for the Right Ventricle

Similar to that for the LV, the VRG can be derived for the RV. Figure 8.4 shows the results based on a study by Holt [18], where heart rate (range 70–108 beats per minute) is reflected by “bubble” size. Average fractional emptying (an expression coined by Holt, nowadays called EF) amounted to 39% for the RV in seven anesthetized dogs, while in a preceding study [16], 46% was found for the LV. Although the authors recognized the fractional behavior of the dilution curves, their primary interest was not EF or any equivalent thereof but rather the estimation of residual volume, i.e., ESV. The findings for the RV VRG shown in Fig. 8.4 have been confirmed in numerous other studies, including, e.g., those reporting on post-Falloff repair studies [28].

The Case of Sharing a Pizza

Imagine that someone offers you a slice of pizza. She or he cuts a piece that is $3/5$ (60%) of the total size. Now, how many bites do you get? Is this going to be a complete meal or just a snack? Well, apart from the toppings, it all depends on whether we are talking about a mini-pizza or a supersized one. So, given the fraction offered, you need to know the circumference (or diameter), because traditional pizzas, homemade or not, are reported to be round. A similar unspecified attribute is involved when discussing EF, which is often magically endowed with the prestigious title: indicator of systolic function.

The metric EF is also often referred to as an index. Wheelan [58] has nicely described how to view such an indicator: “The advantage of any index is that it consolidates lots of complex information into a single number. We can then rank things that otherwise defy simple comparison – anything from quarterbacks to colleges to beauty pageant contestants. In the Miss America pageant, the overall winner is a combination of five separate competitions: personal interview, swimsuit, evening wear, talent, and onstage question.” He continues providing a similar example on ranking sports cars, emphasizing that each classification system has the potential to produce a different outcome. The same line of reasoning applies to the heart when we consider EF.

Robotham et al. [46] concluded: “Thus, EF, although a relatively simple measure that is intuitively easily comprehended, is an extremely complex parameter describing the entire cardiovascular system and requires additional study.” Strictly speaking, the outcome for EF only depends on ESV and EDV when employing the more insightful variant of the definition formula:

$$EF = 100 * (1 - ESV/EDV) \quad (8.1)$$

However, both ESV and EDV themselves depend on many underlying factors. Ventricular function can be described via the volume regulation graph (VRG) approach or based on the elastance concept [27]. ESV and EDV can be related [21] to each other via

$$ESV = \alpha + \beta EDV \quad (8.2)$$

and graphically represented in the VRG; see Fig. 8.4. In the past, we derived an analytical expression by combining Eq. (8.1) with the definition formula for EF:

$$EF = 1 + C_1 \{ESV/(C_2 - ESV)\} \quad (8.3)$$

with constants C_1 and C_2 calculated for the population under consideration (Kerkhof 1984) [21]. This expression underscores the importance of measuring ESV [29, 30]. From the PV loop (Fig. 8.3), we can define (assuming linearity when considering a sufficiently small ESV range) the E_{max} using ESP, end-systolic volume (ESV), and the intercept V_0 [6]:

$$E_{max} = ESP/(ESV - V_0) \text{ or,} \\ ESV = ESP/E_{max} + V_0.$$

The ventricular diastolic stiffness is traditionally defined as an exponential curve [27], by relating end-diastolic pressure (EDP) to two constants (i.e., P_0 and m), $EDP = P_0 e^{(m * EDV)}$, where P_0 is a constant and m is the modulus referring to LV distensibility. Thus, EDV can be expressed as $EDV = (\log EDP - \log P_0)/m$. As a consequence, EF can be described either as a

function of {ESV, ESP, V_0 , EDP, P_0 , and m } or as dependent on {ESV, α , β , R^2 , EDV_{ave} }.

Importantly, the VRG can be used as a starting point to derive various connections with clinically relevant metrics, such as EF and E_{max} . This view is summarized in Fig. 8.5, where (1-EF) is shown by the line connecting the origin with any particular operating point of {EDV, ESV}, for example, for the average values in males and females. In dogs of various breeds, admitted to the clinic because of heart disease, age seems to affect ventricular volume regulation (as reflected by the slope difference in the VRG), but this effect is only discernible in female dogs [42].

Another application of the VRG concept refers to EF versus ESV_i (Fig. 8.6). The male/female regression curves based on Eq. (8.3) show overlap, but average values for males and females are significantly different (Table 8.1).

These findings can be summarized as shown in Fig. 8.7 where EF is presented in the VRG as a box which contains several surprises when we look at the true contents. The example is based on data ($N = 12$) obtained in healthy individuals [1], illustrating that EF is inversely associated with both ESV_i , and with the VAC index, the latter only when assuming that $V_0 = 0$. It is important to note that EF and VAC are “uncoupled” when the true V_0 is taken into account. Otherwise, the relation between EF and VAC is trivial, and one metric does not offer any additional information to that of the other.

Associations Between Clinically Relevant Variables

The insightful and telling Fig. 8.8 obtained from Ky et al. [35] nicely summarizes the associations between major variables of relevance in cardiovascular studies. These authors did not stratify for sex but report that their analysis is based on 466 patients (37% females) with systolic HF with an average EF of 27%. In an earlier study concerning HF patients, we found that both average EF and VAC are significantly higher in women [26]. Table 8.1 documents that this is also the case in

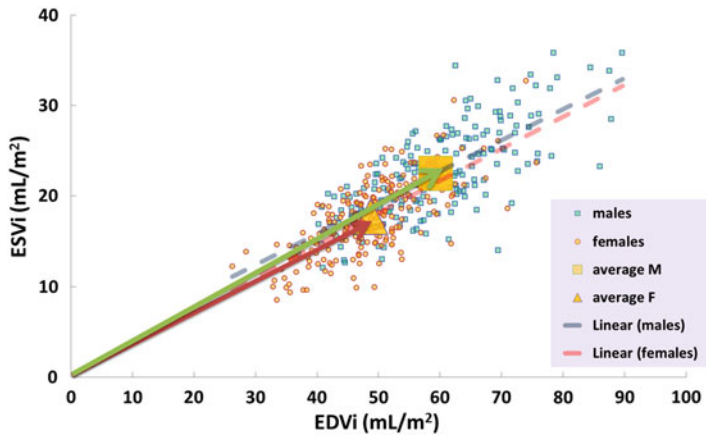
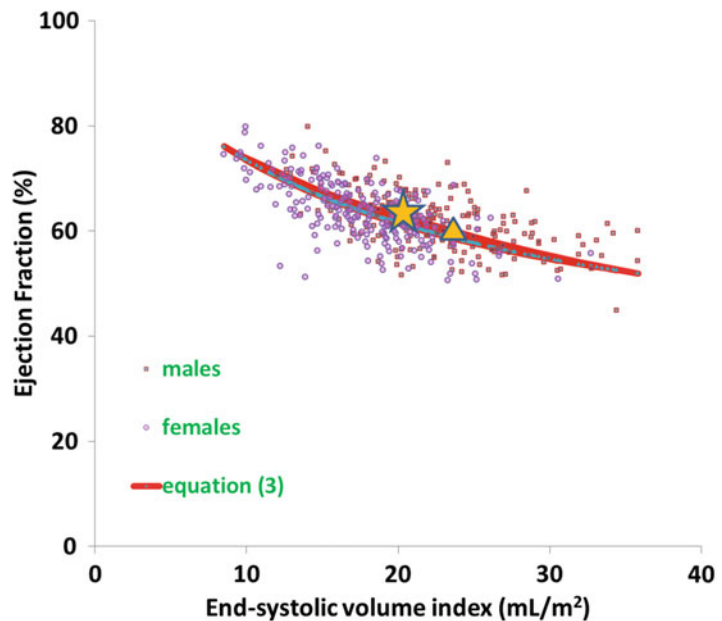


Fig. 8.5 Volume regulation graph, showing relationship between end-systolic volume index (ESVi) and end-diastolic volume index (EDVi) in healthy adult individuals (N = 410), stratified for sex (215 women). The broken lines refer to linear regression analysis. These lines should

be distinguished from the solid lines with arrow heads that connect the origin with each group average, illustrating that average ejection fraction (EF) is higher in women (see Table 8.1). A steeper slope indicates a lower EF. Data from Kuznetsova et al. [34], measured by 2D echocardiography

Fig. 8.6 Ejection fraction (EF) versus end-systolic volume index (ESVi) for healthy individuals, stratified for sex, as also shown in Fig. 8.1. The yellow triangle refers to the average value for males, while the yellow star reflects average value for females. Both EF and ESVi are significantly different (see Table 8.1). The regression curve is based on Eq. (8.3)



healthy adults. Not all variables listed in Fig. 8.8 were discussed in the present survey, but clearly the correlation reported between ESV and EDV is the highest found among all combinations. This outcome supports our starting point reflected by the VRG (Figs. 8.4 and 8.5), which has also been discussed elsewhere [5, 25].

Discussion

Strictly speaking, any sex-specific analysis is of limited meaning if not interpreted against the context of the potential role which age plays. The data we discussed here refer to healthy adults,

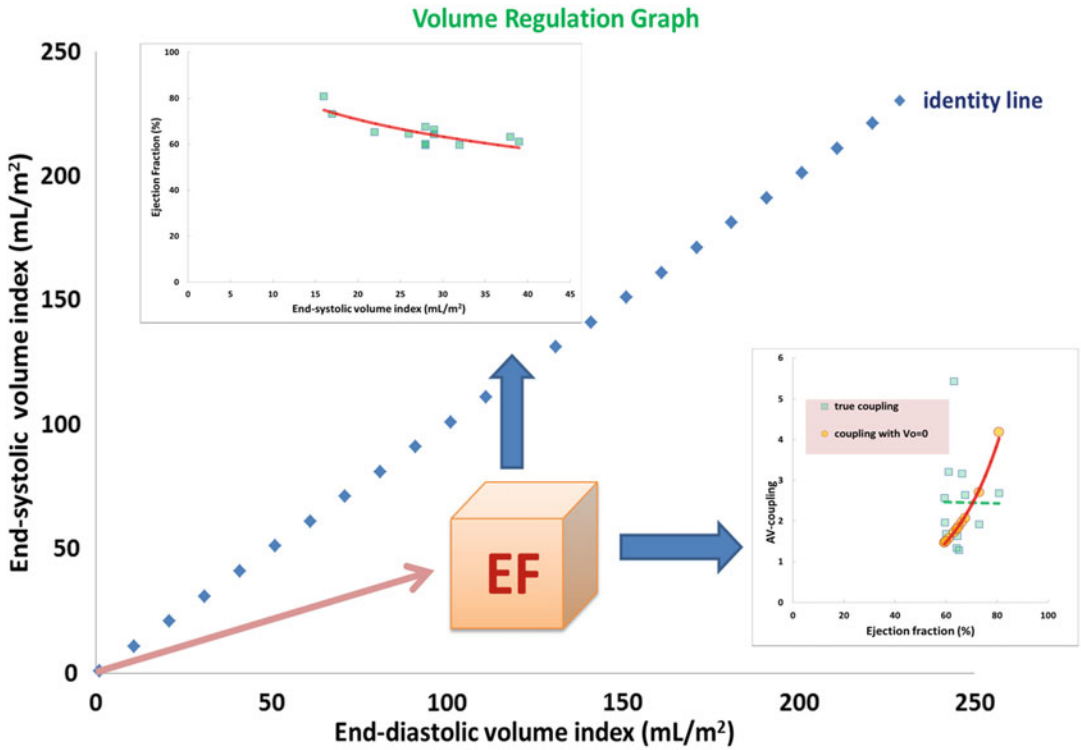


Fig. 8.7 Volume regulation graph illustrating the derivation of ejection fraction (EF) by considering the slope of the line which connects the origin with the pertaining working point defined by {EDV,ESV}. The inset (upper panel) shows that EF is nonlinearly related to ESVi, while

an exponential relationship describes ventriculo-arterial coupling versus EF (lower right inset). For explanation see text. Data (N = 12) based on healthy individuals described by Asanoi et al. [1]

with age ranging from 15 to 90 years. From our observations on healthy adults, we conclude that there are significant sex differences regarding average LV size when considering the nearly complete adult lifespan. These findings fully support earlier findings reported in the literature [8], which unfortunately did not receive the attention it deserves within the clinical discipline. The results on the LV have been extended to the RV, e.g., by [37].

Using gated myocardial perfusion SPECT for the LV, Peace et al. [41] studied the effect of sex, age (range), and weight (range) on LV EF and ESV reference limits in adults. These authors fully confirm the findings obtained by Buonanno et al. [8]. Using coronary CT angiography, Gebhard et al. [12] analyzed 1155 individuals (54.5% males) free from overt heart disease

and found that average EF was 2.0% points higher in females ($p < 0.001$). This male/female difference increased with advancing age (range 18–92 years). Slight age-dependent variation has been observed in some studies, and this potential modifying effect requires further study, because conflicting results have been reported, e.g., no correlation between EF and age [41].

Why ventricular size is generally smaller in healthy females compared to males is not entirely clear. Various factors have been implicated, including differences in neurohumoral signaling, age-dependent changes in estrogen/progesterone status, gender-related life style factors, and progressive cardiomyocyte loss with age in males (but not observed in women).

The embryologic origins of the RV and the LV differ. The RV exhibits dominant pump function

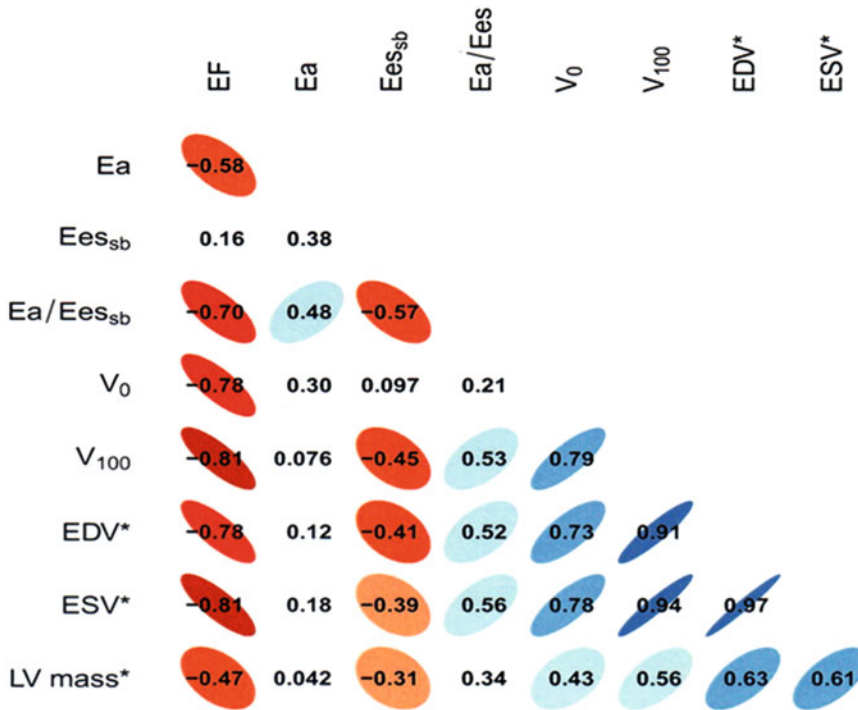


Fig. 8.8 Cross table of volume-related variables of the left ventricle, measured by echocardiography in 466 patients with chronic systolic heart failure, showing correlation coefficients for all combinations of two components. Ees is obtained by the single beat (sb) method and more or less comparable to E_{max} in our text. Note that the coupling index is here defined as our (k⁻¹). The blue ellipse signifies a positive correlation, while a red contour refers

to negative correlation. The intensity of the color reflects the strength of the association. Interestingly, the two variables which we employ for depicting the volume regulation graph, namely, ESV and EDV, yield the highest correlation. V₁₀₀ is the volume which corresponds with a pressure level of 100 mmHg on the linearized E_{max} curve. Abbreviations as in our text. Reproduced from Ky et al. [35], with permission

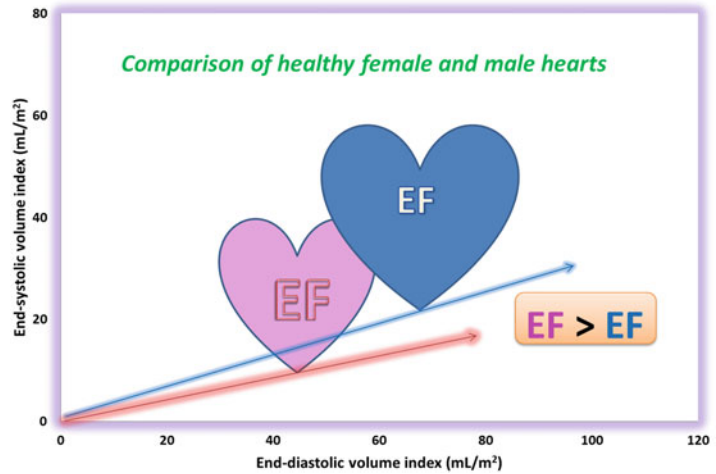
during fetal development. At birth, separation of the pulmonary and the systemic circulation causes that the LV assumes primary pump function generating much higher needed pressures. Concomitant with morphological and functional modifications in both the LV and RV, the neonatal cardiomyocytes undergo changes in morphology, respiration, metabolism, and contractile function. Distinct key transcription factors drive the chamber-specific gene networks during development. Existing evidence reveals a critical role of noncanonical Wnt11 in orchestrating early development. Expression of Wnt11 is dynamically regulated in a temporal-spatial manner, playing important roles in myocardial development [55]. However, these researchers only looked at male mice, and further investigations are needed.

Another intriguing approach for elucidating male/female phenotypic differences in cardiac size follows the pattern of ventricular volume adaptation for sex-mismatch cases in heart transplant patients, both in children and adults [43].

Conclusions

In healthy adults we observe striking (significant) differences when blood pressure and left ventricular volumes are compared in males and females. These disparities have serious consequences for particular metrics commonly used to evaluate cardiovascular function. Pulse pressure (which is related to vascular stiffness) is higher in males. In contrast EF (often used to assess systolic

Fig. 8.9 Summary of dimensional findings regarding left ventricular size in healthy adult women and men. Ejection fraction (EF) is generally higher in smaller hearts (as in women), because end-systolic volume index (ESVi) tends to be smaller, while end-diastolic volume index “follows” ESVi. Schematic dimensions of the symbolic heart are somewhat exaggerated to make this point clearly visible



function), E_{max} (reflecting contractility), and VAC are higher in women (assuming that the intercept V_0 can be neglected). However, mean blood pressure (an indicator of afterload) is lower in women. As illustrated, ESV and EDV are linearly correlated, clarifying why EF is slightly higher in women (Figs. 8.4 and 8.9), and permitting the robust description of various relationships, including EF vs ESV(i). It is often emphasized that sex matters when studying cardiovascular properties, and this notion has been confirmed in the present analysis based on healthy individuals. Further studies in cardiac disease patients are required to investigate if these differences persist in selected diagnostic cohort categories and what ultimately will be the implications for more precise diagnosis and treatment.

References

- Asanoi H, Sasayama S, Kameyama T. Ventriculoarterial coupling in normal and failing heart in humans. *Circ Res.* 1989;65:483–93.
- Ayaz O, Howlett SE. Testosterone modulates cardiac contraction and calcium homeostasis: cellular and molecular mechanisms. *Biol Sex Differ.* 2015;6:9. <https://doi.org/10.1186/s13293-015-0027-9>.
- Baan J, Jong TT, Kerkhof PL, Moene RJ, van Dijk AD, van der Velde ET, Koops J. Continuous stroke volume and cardiac output from intra-ventricular dimensions obtained with impedance catheter. *Cardiovasc Res.* 1981;15:328–34.
- Bataille G. The cradle of humanity, prehistoric art and culture. New York: Zone Books; 2009.
- Beringer JY, Kerkhof PLM. A unifying representation of ventricular volumetric indexes. *IEEE Trans BME.* 1998;45:365–71.
- Blaudszun G, Morel DR. Relevance of the volume-axis intercept, V_0 , compared with the slope of end-systolic pressure-volume relationship in response to large variations in inotropy and afterload in rats. *Exp Physiol.* 2011;96:1179–95.
- Buonanno C. The female left ventricle: a pathophysiological entity? *Int J Cardiol.* 1983;4:382–6.
- Buonanno C, Arbustini E, Rossi L, Dander B, Vassanelli C, Paris B, Poppi A. Left ventricular function in men and women. Another difference between sexes. *Eur Heart J.* 1982;3:525–8.
- Coronado MJ, Fairweather D, Bruno KA. Sex determines cardiac myocyte stretch and relaxation. *Circ Cardiovasc Genet.* 2017;10(5):e001950.
- Farrell SR, Ross JL, Howlett SE. Sex differences in mechanisms of cardiac excitation-contraction coupling in rat ventricular myocytes. *Am J Physiol Heart Circ Physiol.* 2010;299:H36–45. <https://doi.org/10.1152/ajpheart.00299.2010>.
- Fazal L, Azibani F, Vodovar N, Cohen Solal A, Delcayre C, Samuel JL. Effects of biological sex on the pathophysiology of the heart. *Br J Pharmacol.* 2014;171:555–66. <https://doi.org/10.1111/bph.12279>.
- Gebhard C, Buechel RR, Stähli BE, Gransar H, Achenbach S, Berman DS, et al. Impact of age and sex on left ventricular function determined by coronary computed tomographic angiography: results from the prospective multicentre CONFIRM study. *Eur Heart J Imag.* 2017;18:990–1000.
- Hales S. Statical essays. London: Innys & Co; 1733. See also http://www.bg.ic.ac.uk/research/k.parker/wave_intensity_web/history_hales.htm
- Harvey W. Exercitatio anatomica de motu cordis et sanguinis in animalibus. Frankfurt a Main: W. Fitzer; 1628.
- Helmes M, Lim CC, Liao R, Bharti A, Cui L, Sawyer DB. Titin determines the Frank-Starling relation in early diastole. *J Gen Physiol.* 2003;121:97–110.
- Holt JP. Estimation of the residual volume of the ventricle of the dog's heart by two indicator dilution technics. *Circ Res.* 1956;4:187–95.

17. Holt JP. Regulation of the degree of emptying of the left ventricle by the force of ventricular contraction. *Circ Res.* 1957;5:281–7.
18. Holt JP, Allensworth J. Estimation of the residual volume of the right ventricle of the dog's heart. *Circ Res.* 1957;5:323–6.
19. Huxley AF. Muscle structure and theories of contraction. *Prog Biophys Biophys Chem.* 1957;7:255–318.
20. Kajstura J, Gurusamy N, Ogórek B, et al. Myocyte turnover in the aging human heart. *Circ Res.* 2010;107:1374–86. <https://doi.org/10.1161/CIRCRESAHA.110.231498>.
21. Kerkhof PLM. Importance of end-systolic volume for the evaluation of cardiac pump performance. In: Chazov EI, Smirnov VN, Oganov RG, editors. *Cardiology, an international perspective.* New York: Plenum Press; 1984. p. 1339–52.
22. Kerkhof PLM. Combination of Millar and conductance catheter to assess equine left ventricular function. In: Conference Proceedings: annual International Conference of the IEEE Engineering in Medicine and Biology Society, Atlanta. 1999.
23. Kerkhof PLM. Fundamentals of left ventricular volume representation. *Conf Proc IEEE Eng Med Biol Soc.* 2016Aug;2016:3294–3297. doi: <https://doi.org/10.1109/EMBC.2016.7591432>. PMID: 28227221.
24. Kerkhof PLM. Physiological modeling survey. In: Webster J, editor. *Encyclopedia of electrical and electronics engineering.* 3rd revised ed. New York: Wiley; 2018.
25. Kerkhof PLM, Kresh JY, Li JK-J, Heyndrickx GR. Left ventricular volume regulation in heart failure with preserved ejection fraction. *Physiol Rep.* 2013;1:e00007.
26. Kerkhof PLM, Heyndrickx GR, Li JK. Hemodynamic determinants and ventriculo-arterial coupling are sex-associated in heart failure patients. *Conf Proc IEEE Eng Med Biol Soc.* 2016Aug;2016:3286–3289. doi: <https://doi.org/10.1109/EMBC.2016.7591430>. PMID: 28227219.
27. Kerkhof PLM, Yoo BW, Merillon JP, Peace RA, Handly N. Monte Carlo method applied to the evaluation of the relationship between ejection fraction and its constituent components. *Conf Proc IEEE Eng Med Biol Soc.* 2017a;2017:1295–8. <https://doi.org/10.1109/EMBC.2017.8037069>.
28. Kerkhof PLM, Yoo BW, van de Ven PM, Handly N. Sex-specific aspects of left and right ventricular volume regulation in patients following tetralogy of Fallot repair. *Conf Proc IEEE Eng Med Biol Soc.* 2017b;2017:1303–6. <https://doi.org/10.1109/EMBC.2017.8037071>.
29. Kerkhof PLM, Peace RA, Handly N. The importance of (measuring) the end-systolic volume index in predicting survival. *Heart.* 2018a;104:180. <https://doi.org/10.1136/heartjnl-2017-312051>.
30. Kerkhof PLM, van de Ven PM, Yoo BW, Peace RA, Heyndrickx GR, Handly N. Ejection fraction as related to basic components in the left and right ventricular volume domains. *Intern J Cardiol.* 2018b;255:105–10.
31. Kerkhof PLM, Heethaar RM, Pearce JA. Bioimpedance: principles, measurements, and applications. In: Webster J, editor. *Encyclopedia of electrical and electronics engineering.* 3rd revised ed. New York: Wiley; 2018c.
32. Kerkhof PLM, Kuznetsova T, Ali R, Handly N. Left ventricular volume analysis as a basic tool to describe cardiac function. *Adv Physiol Educ.* 2018d;42(1):130–139. doi: <https://doi.org/10.1152/advan.00140.2017>.
33. Kulpa J, Chinnappareddy N, Pyle WG. Rapid changes in cardiac myofibrillar function following the acute activation of estrogen receptor- α . *PLoS One.* 2012;7(7):e41076. <https://doi.org/10.1371/journal.pone.0041076>.
34. Kuznetsova T, Haddad F, Tikhonoff V, et al. Impact and pitfalls of scaling of left ventricular and atrial structure in population-based studies. *J Hypertens.* 2016;34:1186–94.
35. Ky B, French B, May Khan A, Plappert T, Wang A, Chirinos JA, et al. Ventricular-arterial coupling, remodeling, and prognosis in chronic heart failure. *J Am Coll Cardiol.* 2013;62:1165–72.
36. *Lancet* October 5, 1974.
37. Maffessanti F, Muraru D, Esposito R, Gripari P, Ermacora D, Santoro C, et al. Age-, body size-, and sex-specific reference values for right ventricular volumes and ejection fraction by three-dimensional echocardiography: a multicenter echocardiographic study in 507 healthy volunteers. *Circ Cardiovasc Imaging.* 2013;6:700–10.
38. Mazzoni M. Dario Maestrini e la legge del cuore Storia di un mancato Premio Nobel. *Notizie dalla Delfico.* 2005; 1–2. See also [http://www.treccani.it/enciclopedia/dario-maestrini_\(Dizionario-Biografico\)/](http://www.treccani.it/enciclopedia/dario-maestrini_(Dizionario-Biografico)/)
39. Negroni JA, Morotti S, Lascano EC, Gomes AV, Grandi E, Puglisi JL, Bers DM. β -adrenergic effects on cardiac myofilaments and contraction in an integrated rabbit ventricular myocyte model. *Mol Cell Cardiol.* 2015;81:162–75.
40. Parks RJ, Howlett SE. Sex differences in mechanisms of cardiac excitation-contraction coupling. *Pflugers Arch.* 2013 May;465(5):747–63. doi: <https://doi.org/10.1007/s00424-013-1233-0>
41. Peace RA, Adams PC, Lloyd JJ. Effect of sex, age, and weight on ejection fraction and end-systolic volume reference limits in gated myocardial perfusion SPECT. *J Nucl Cardiol.* 2008;15:86–93.
42. Pijnenburg HLM, Kerkhof PLM, Kocsis S, Voorhout G. Ventricular volume regulation in dogs as a function of gender, age and breed. *FASEB J.* 1996;10:A346.
43. Previato M, Kerkhof PLM, Osto E, Parry G, Tona F. Heart transplantation survival and sex-related differences. In: Kerkhof PLM, Miller VM, editors. *Sex-specific analysis of cardiovascular function.* New York: Springer; 2018.
44. Puglisi JL, Negroni JA, Chen-Izu Y, Bers DM. The force-frequency relationship: insights from mathematical modeling. *Adv Physiol Educ.* 2013;37:28–34.
45. Putschner M. *Geschichte der medizinischen Abbildung.* Heinz Moos Verlag: Muenchen; 1972.
46. Robotham JL, Takata M, Berman M, Harasawa Y. Ejection fraction revisited. *Anesthesiology.* 1991;74(1):172–83.
47. Sakai S. Jacob Berengario. *Igaku Toshokan.* 1986;33:29–31. <https://doi.org/10.7142/igakutoshokan.33.29> [The Japan Medical Library Association].
48. Sandberg K, Ji H. Sex differences in primary hypertension. *Biol Sex Differ.* 2012;3:7. <https://doi.org/10.1186/2042-6410-3-7>.
49. Sequeira V, van der Velden J. Historical perspective on heart function: the Frank–Starling law. *Biophys Rev.* 2015;7:421–47.
50. Shannon TR, Wang F, Puglisi J, Weber C, Bers DM. A mathematical treatment of integrated ca dynamics within the ventricular myocyte. *Biophys J.* 2004;87:3351–71.
51. Sharma K, Kass DA. Heart failure with preserved ejection fraction: mechanisms, clinical features, and therapies. *Circ Res.* 2014;115:79–96.
52. Shavik SM, Wall ST, Sundnes J, Burkhoff D, Lee LC. Organ-level validation of a cross-bridge cycling descriptor in a left ventricular finite element model: effects of ventricular loading on myocardial strains. *Physiol Rep.* 2017;5(21):e13392. <https://doi.org/10.14814/phy2.13392>.
53. Singer C. *A short history of anatomy and physiology from the Greeks to Harvey.* New York: Dover Publications; 1957.

54. Soltis AR, Saucerman JJ. Synergy between CaMKII substrates and β -adrenergic signaling in regulation of cardiac myocyte Ca(2+) handling. *Biophys J*. 2010;99:2038–47.
55. Touma M, Kang X, Gao F, Zhao Y, Cass AA, Biniwale R, Xiao X, Eghbali M, Coppola G, Reemtsen B, Wang Y. Wnt11 regulates cardiac chamber development and disease during perinatal maturation. *JCI Insight*. 2017;2(17):94904.
56. Trexler CL, Odell AT, Jeong MY, Dowell RD, Leinwand LA. Transcriptome and functional profile of cardiac myocytes is influenced by biological sex. *Circ Cardiovasc Genet*. 2017;10(5):e001770. <https://doi.org/10.1161/CIRCGENETICS.117.001770>.
57. Van Liere EJ, Stickney JC, Marsh DF. Sex differences in blood pressure of dogs. *Science*. 1949;109:489.
58. Wheelan C. *Naked statistics*. New York: WW Norton; 2013.